Evolution of the Amyloid Fiber over Multiple Length Scales

Devin M. Ridgley and Justin R. Barone*

Biological Systems Engineering Department, Virginia Tech, 303 Seitz Hall, Blacksburg, Virginia 24061, United States

ABSTRACT The amyloid is a natural self-assembled peptide material comparable in specific stiffness to spider silk and steel. Throughout the literature there are many studies of the nanometer-sized amyloid fibril; however, peptide mixtures are capable of self-assembling beyond the nanometer scale into micrometer-sized fibers. Here, atomic force microscopy (AFM) and scanning electron microscopy (SEM) are used to observe the self-assembly of the peptide mixtures in solution for 20 days and the fibers upon drying. Beyond the nanometer scale, self-assembling fibers differentiate into two morphologies, cylindrical or rectangular cross-section, depending on peptide properties. Microscopic observations delineate a four stage self-assembly mechanism: (1) protofibril (2—4 nm high and 15—30 nm wide) formation; (2) protofibril aggregation into fibrils 6—10 nm high and 60—120 nm wide; (3) fibril aggregation into large fibrils and morphological differentiation where large fibrils begin to resemble the final fiber morphology of cylinders (WG peptides) or tapes (Gd:My peptides). WG large fibrils are 50 nm high and 480 nm wide and Gd:My large fibrils are 10 nm high and 150 nm wide; (4) micrometer-sized fiber formation upon drying at 480 h resulting in 18.0 μm diameter cylindrical fibers (WG peptides) and 14.0 μm wide and 6.0 μm thick flat tapes (Gd:My peptides). Evolution of the large fiber morphology can be rationalized on the basis of the peptide properties.

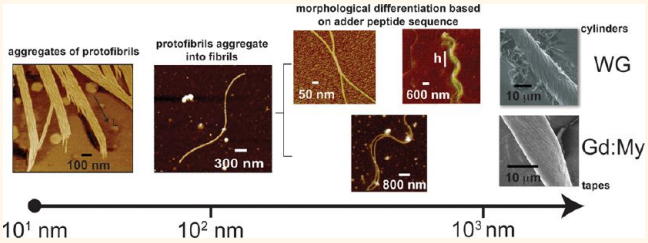

KEYWORDS: self-assembly · protein · cross-β structure · amyloid · fibril · fiber

Amyloids are self-assembled protein materials containing β-sheets.[1−4] There is a large body of work focused on amyloids in pathogenic "prion" diseases such as Alzheimer's, Parkinson's, and Huntington's Diseases.[1,3−5] Self-assembly begins when a protein molecule "misfolds", straightens out, and hydrogen bonds to another misfolded, straight protein molecule to build the β-sheet. Thus these diseases are also termed "protein misfolding diseases". It is now believed that this small β-sheet aggregate is the pathogenic structure in disease pathology. These small β-sheet aggregates can continue to aggregate into protofibrils with diameters of 1−10 nm and lengths of >100 nm. Several protofibrils can then aggregate together into the prion "plaques" observed in advanced prion disease.[6] In amyloid fibrils, the protein chain axis is perpendicular to the fibril axis and thus the β-sheets are termed "cross-β" sheets. In contrast, the protein chain axis and resulting β-sheets in natural silk and β-keratin fibers are aligned along the fiber axis. This is because of the applied deformation required to form the silk or β-keratin fiber, that is, spinning or extrusion. The cross-β structure can be differentiated from β-sheets aligned along the fiber using vibrational spectroscopy or X-ray diffraction.[7,8]

Not all amyloids are detrimental structures. Nature is able to produce a class of beneficial self-assembled structures known as "functional" amyloids meant to proliferate life.[3,9,10] Barnacle cement has been shown to be a rigid, strong, and tough adhesive because it is a composite of insoluble cross-β fibrils in a protein matrix.[11−15] The bacterium *Streptomyces coelicolor* and fungus *Neurospora crassa* self-assemble proteins into extracellular amyloid fibrils and hyphae, respectively, for adhesion and biofilm formation.[10,16] *Escherichia coli* will secrete curli proteins CsgA and CsgB to form fibrous amyloids on the cell surface.[17−21] Cell adhesion proteins on *Candida albicans* form rigid amyloid fibers.[22] Insects of the *Chrysopidae* family form cross-β silks to suspend their eggs for protection.[23,24]

The fibrous amyloid is similar in rigidity to other β-sheet containing protein fibers and the specific modulus approaches that of steel.[25−27] Thus, very rigid materials are

* Address correspondence to jbarone@vt.edu.

Received for review August 2, 2012 and accepted December 23, 2012.

Published online December 26, 2012
10.1021/nn303489a

formed from a host of weak hydrogen bonds. It has been shown that β-sheets confined to a few nanometers achieve higher modulus, strength, and toughness than larger β-sheets.[28] The smaller β-sheets, about 3 nm in size, give a stick−slip shear response to applied deformation, whereas larger β-sheets, about 7 nm in size, bend. Young's modulus calculated from molecular dynamics and density functional theory yield values of 22.6 and 36.5 GPa, respectively, which agree well with experiment.[26] Thus the size and hierarchy of β-sheet structures in the amyloid influences the properties. Amyloid fibrils have also shown great solvent and temperature resistance, and the fact that no known cure exists for prion disease is a testament to the robustness of the self-assembled β-sheet structure.[29] The outstanding physical properties and observed functional role of amyloids in nature serve as inspiration to use the self-assembled structures as high performance biomaterials in unique nanodevices and nanocomposites.[30−34]

Nanometer-sized amyloid fibrils can spontaneously self-assemble from a host of proteins and peptides.[9,30,35−43] Past studies have documented the growth and morphological development of the nanometer-sized amyloid fibril under various conditions.[34,37,43−69] It is generally accepted that any protein is capable of self-assembling into an amyloid fibril given the right conditions, which are usually extremely denaturing.[3,4] Several studies have implicated a nucleation site or seed in order for amyloid formation to occur.[70,71] Amyloid fibril size is dependent on the peptide or protein used and has been shown to be about 2−10 nm wide with some larger structures forming through aggregation of smaller structures.[40,63,72,73] Solution conditions can also affect the amyloid fibril size and morphology.[74−76] Adamcik *et al.* were able to self-assemble multiple fibrils into twisted tapes with adjustable pitches based on the solution NaCl concentration.[64] The highly studied Aβ(1−40) peptide implicated in prion disease can aggregate into β-structured polymorphs ranging from amorphous aggregates to fibril morphologies by varying NaCl, Zn^{2+}, and SDS concentrations in the incubating solutions.[77]

Fibers larger than nanometer-sized fibrils have been predicted in several studies.[40,78−80] Tapes composed of fibrils can be self-assembled up to approximately 150 nm in width.[81] Recent research has shown that it is possible to self-assemble micrometer-sized amyloid fibers from peptide mixtures.[35,36,75] This mechanism is similar to a previous hypothesis that requires a nucleation site or seed for initiation of cross-β formation and fibril growth.[70,82,83] Extensive research into the self-assembly of fibrils on the nanometer scale has been performed; however, little is understood about the mechanism of self-assembly beyond the nanometer scale, especially in terms of how self-assembling peptide systems can morphologically differentiate beginning at smaller scales and how the morphology persists to higher scales. Here, two peptide mixtures, hydrolyzed wheat gluten (WG) and hydrolyzed gliadin:unhydrolyzed myoglobin (Gd:My), are monitored in solution for 20 days with atomic force microscopy (AFM) and upon drying with scanning electron microscopy (SEM) to elucidate the mechanism for self-assembly of amyloid fibers from the molecular to the micrometer scale. Differences between the peptides in the two mixtures manifest at the nanometer scale and continue through the hierarchy to produce micrometer-sized fibers and tapes with different properties and morphologies. Hierarchical micrometer-sized fibers are the structural material of choice in nature. This research shows that peptide systems can be designed at the molecular level to produce useful, large-scale biomimetic materials that are predictable and controllable.

RESULTS AND DISCUSSION

Trypsin-hydrolyzed wheat gluten and gliadin produce a mixture of peptides that can be used for self-assembly over several orders of magnitude of scale. Wheat gluten is a combination of gliadin and glutenin proteins and replacing the hydrolyzed glutenin fraction with unhydrolyzed myoglobin produces a tape rather than a fiber.[35] Although the hydrolysis produces several peptides, only certain peptides in the mixture have a propensity to self-assemble.[35,75] Those peptides have since been individually synthesized and mixed together and with myoglobin producing similar results to the crude mixture.[35] In the proposed mechanism, a hydrophobic "template" peptide forms a cross-β template to hide hydrophobic amino acid side groups in spaces between β-sheets. The template peptide has hydrophobic amino acids residing next to one another and thus has some hydrophobic groups exposed to the water on the outer faces of the β-sheets (Scheme 1, Stage I). Hydrolyzed gliadin produces the template peptide, Gd20.[35] The "adder" peptide or protein is α-helical and less hydrophobic than the template peptide. A glutenin peptide, GtL75, acts as the adder in the WG system and myoglobin acts as the adder protein in the Gd:My system. The more hydrophilic adder peptide or protein is stable in aqueous solution and does not individually undergo conformation change or aggregate at the experimental conditions as measured with FT-IR spectroscopy.[35,36] However, in the presence of the template, the hydrophobic groups on the α-helices prefer the exposed hydrophobic groups of the template, undergo an α to β transition, and "add" into the template as measured with Fourier transform-infrared (FT-IR) spectroscopy.[35,75] Through AFM and SEM imaging, the progression of large amyloid fiber aggregation can be defined in terms of four morphological stages.

Stage I: Protofibril Formation (*ca.* 0−264 h). WG peptides aggregate into protofibrils $H = 2.5 \pm 0.5$ nm high and

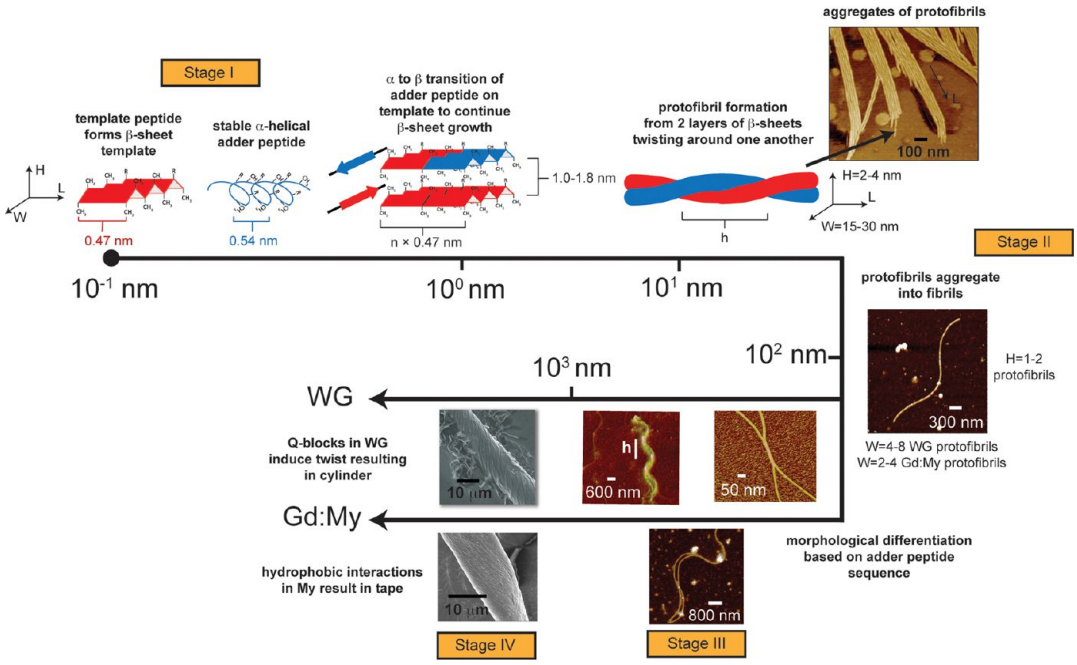

Scheme 1. Four-stage mechanism for peptide mixture aggregation over multiple length scales. In Stage I, the adder peptide is shown adding to the upper β-sheet length and adding to the lower β-sheet height, which are both possible. Morphological differentiation and growth to the micrometer-scale occur in Stages III and IV.

$W = 16.5 \pm 4.5$ nm wide. Gd:My peptides aggregate into protofibrils with $H = 4.3 \pm 1.0$ nm and $W = 31.6 \pm 3.2$ nm with a large protofibril depicted in Figure 1c. X-ray diffraction results show that the protofibril is 2 β-sheet layers high and the distance between sheets is mediated by the largest amino acid side chains.[36] My (17083 g/mol) has a larger molecular weight than GtL75 (8,465 g/mol), and the unassembled chain length also contributes to the observed larger protofibrils.[73] WG protofibrils separate from larger globules while Gd:My protofibrils appear spontaneously (Figure 1c,d). The largest molecular secondary structure transitions occur in Stage I in both WG and Gd:My peptide mixtures.[35]

Stage II: Protofibril Aggregation into Fibrils (*ca.* 240−360 h). Protofibrils aggregate to form larger structures termed fibrils. WG fibrils have $H = 6.7 \pm 2.0$ nm and $W = 82.9 \pm 26.1$ nm (Figure 2a). Gd:My fibrils are $H = 8.6 \pm 2.3$ nm high and $W = 101.0 \pm 28.8$ nm wide (Figures 1c and 2b). FT-IR spectra also reveal an increase in the ratio of the symmetric CH_3 deformation, δ_s, to the asymmetric CH_3 deformation, δ_{as}, throughout the four-stage mechanism. An increase in δ_s/δ_{as} suggests that hydrophobic interactions between peptides play a significant role in conformation change and further self-assembly.[35] Thus, exposed hydrophobic groups on protofibrils continue to hide from water and drive self-assembly. The width of the fibril is composed of 4−8 and 2−4 protofibrils aggregating laterally in the WG and Gd:My systems, respectively. Measured fibril heights are consistent with 1−2 protofibrils aggregating vertically and twisting. Protofibril and fibril formation appear consistent with what has been observed by others where tapes ~2 nm high and 4−10 nm wide form from 2 nm diameter protofibrils aggregating horizontally and twisting[63,64] or "protofilaments" assembling into fibrils in the same manner that protofibrils assemble into fibrils as shown in Figures 1 and 2.[72,73,81,84,85]

The Gd:My fibril structure in Figure 2b resembles the "nanoracket" predicted for Aβ(1−40) fibrils.[6] Gd:My fibrils (also shown in Figure 3) appear to have a lower persistence length, l_p, than WG fibrils and can bend onto themselves. Hydrophobic interactions near the ends of the fibril produce the nanoracket. An estimate of the persistence length for WG and Gd:My Stage II fibrils yields $l_{p,WG} = 1681 \pm 494$ nm and $l_{p,Gd:My} = 1074 \pm 304$ nm. Adamcik *et al.* formed fibrils from the same peptides and found persistence length to scale with the fibril height with thicker fibrils giving a longer persistence length.[63] In Stage II, WG fibrils are narrower and thinner than Gd:My fibrils but possess a longer persistence length, indicating that WG peptides self-assemble into a tighter and more rigid structure. The persistence length is directly proportional to the Young's modulus of the fibril, and thus the Stage II persistence lengths show that property differences between the two systems begin to manifest early in the self-assembly process.

Stage III: Fibril Aggregation into Large Fibrils and Morphological Differentiation (*ca.* 288−480 h). Fibrils aggregate into larger structures termed "large fibrils". WG fibrils twist around each other to form a large fibril with $H = 51.5 \pm 5.8$ nm and $W = 483.5 \pm 30.3$ nm (Figure 3a). The WG large fibril in Figure 2a has $H = 14.0$ nm and $W = 200.0$ nm and shows an intermediate structure

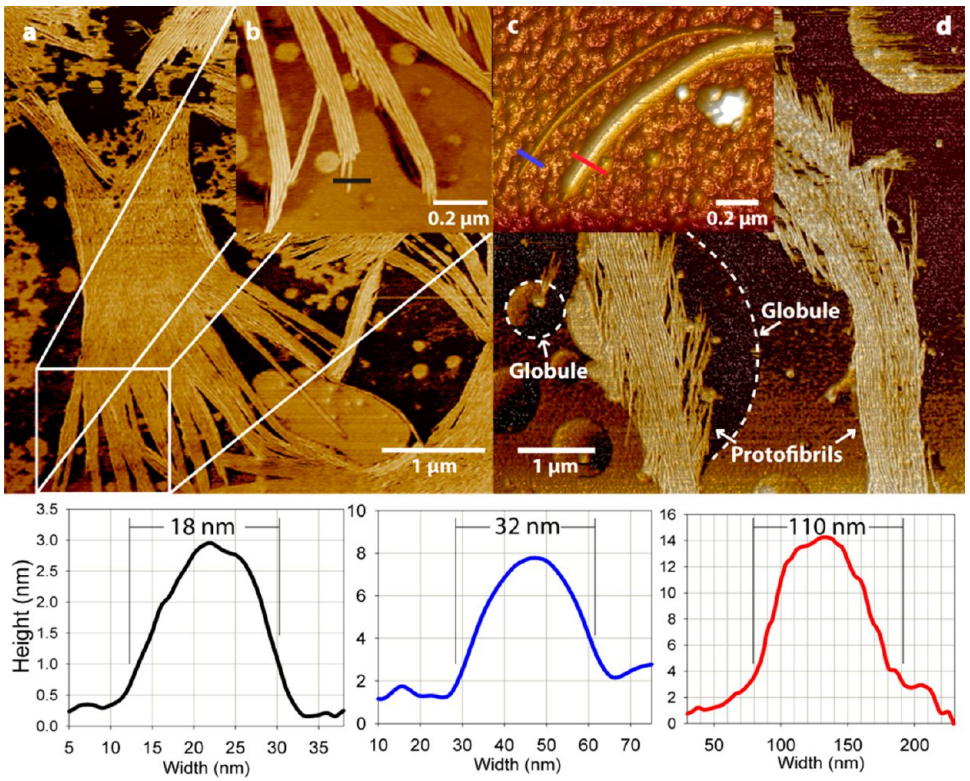

Figure 1. Stage I: (a,b) AFM tapping phase images showing WG aggregated fibrils composed of individual protofibrils of $H = 2.8$ nm and $W = 18.0$ nm (black). (c) AFM topographical image of a large Gd:My protofibril of $H = 6.0$ nm and $W = 32.0$ nm (blue) and fibril of $H = 14.0$ nm and $W = 110.0$ nm (red). (d) AFM tapping phase image of WG fibrils composed of individual protofibrils separating from large globules at very early time.

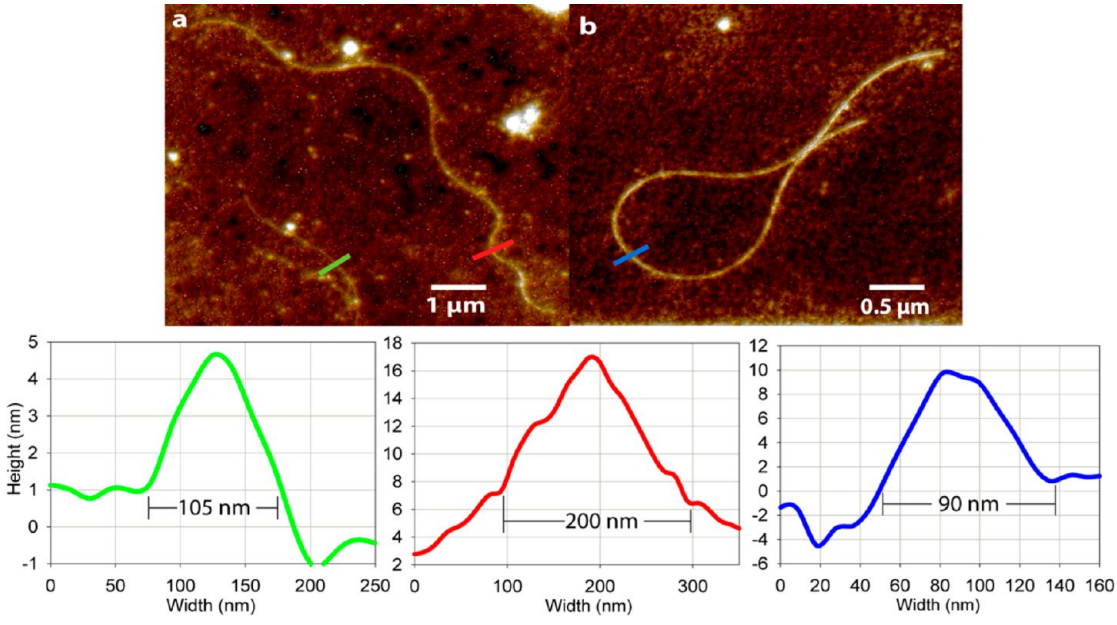

Figure 2. Stage II: AFM topographical images of (a) WG fibril (green) and large fibril (red) and (b) Gd:My fibril (blue).

between Stages II and III. The cross-section is still anisotropic but the beginnings of the final twisted morphology appear in solution at late times. Gd:My fibrils have limited aggregation into large fibrils with $H = 9.8 \pm 1.2$ nm and $W = 155.7 \pm 23.2$ nm (Figure 3b). The final rectangular cross-section of large Gd:My fibers begins in solution and persists upon drying. This is the predominant structure in Stage III.

Morphological differentiation occurs in Stage III where about 4–8 WG fibrils twist into a large fibril

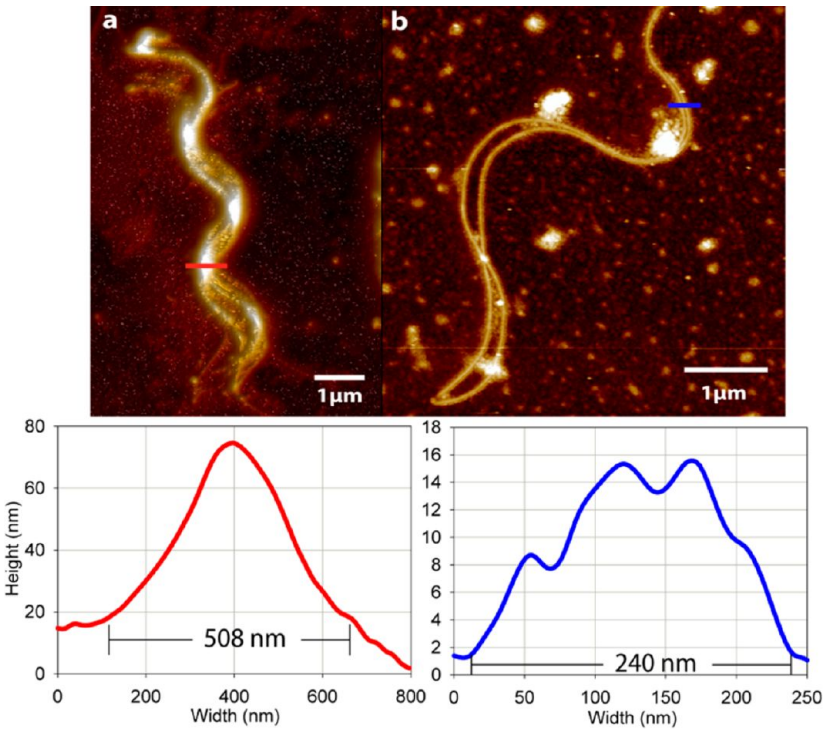

Figure 3. Stage III: AFM topographical images of (a) WG fibrils twisting around each other to form large fibrils and (b) Gd:My fibrils that do not aggregate as frequently or to the same scale as WG fibrils.

with a pitch $h \approx 1410$ nm. The twisting is observable in the AFM image and is confirmed by a large height increase. The WG large fibril is about an order of magnitude smaller than its final fiber dimensions with a pitch about half the length of the final pitch. In Stage III, there is limited Gd:My fibril aggregation into large fibrils resulting in a tape structure with dimensions about an order of magnitude smaller than the final dried tape. Figure 3 shows that Gd:My fibrils have limited lateral aggregation at a stage where WG fibrils begin to twist into a larger structure. Although the morphology of amyloid fibrils at the nanometer scale has been extensively studied, little is known about the continued self-assembly and morphological differentiation at larger scales, which show striking features that can be related to the peptides in the mixtures.[81]

Stage IV: Micrometer-Sized Fiber Formation (>480 h). The final micrometer-sized structure forms upon drying at 480 h. WG peptides form cylindrical fibers of 18.1 ± 9.5 μm in diameter (Figure 4) while Gd:My peptides form flat tapes of $H = 5.7 \pm 0.6$ μm and $W = 14.4 \pm 2.2$ μm (Figure 5). Previous studies using X-ray diffraction and Raman spectroscopy show the WG fibers and Gd:My tapes to contain the cross-β secondary structure.[35,36,75] The final fibers are 10^2-10^3 μm long.[35] Evidence of earlier stage structures exist: WG forms tightly twisted cylindrical cross-section fibers composed of $W = 300-800$ nm wide large fibrils and Gd:My forms rectangular cross-section tapes with $W = 20$ nm protofibrils and $W = 190$ nm large fibrils observed showing the

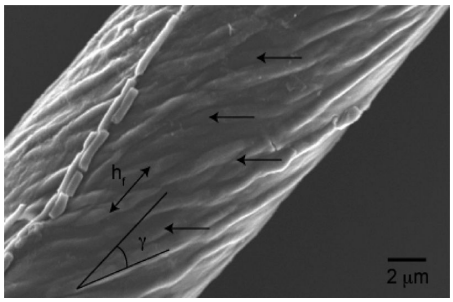

Figure 4. WG fiber of $D = 14.0$ μm composed of twisted large fibrils of 300−800 nm diameter. Arrows indicate where large fibrils twist on top of one another.

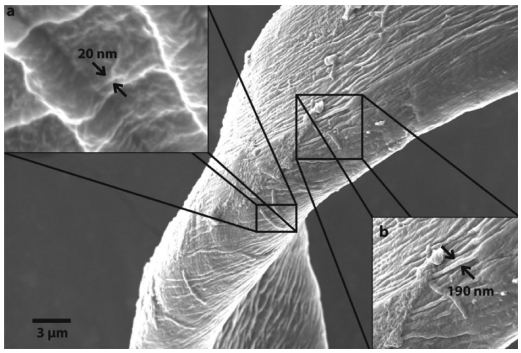

Figure 5. An SEM image of a Gd:My tape ($W = 15$ μm, $H = 6$ μm) where (a) protofibrils and (b) large fibrils are apparent.

micrometer-sized fibers and tapes to be hierarchical. Upon drying the Gd:My solution, large fibrils of $W = 190-900$ nm

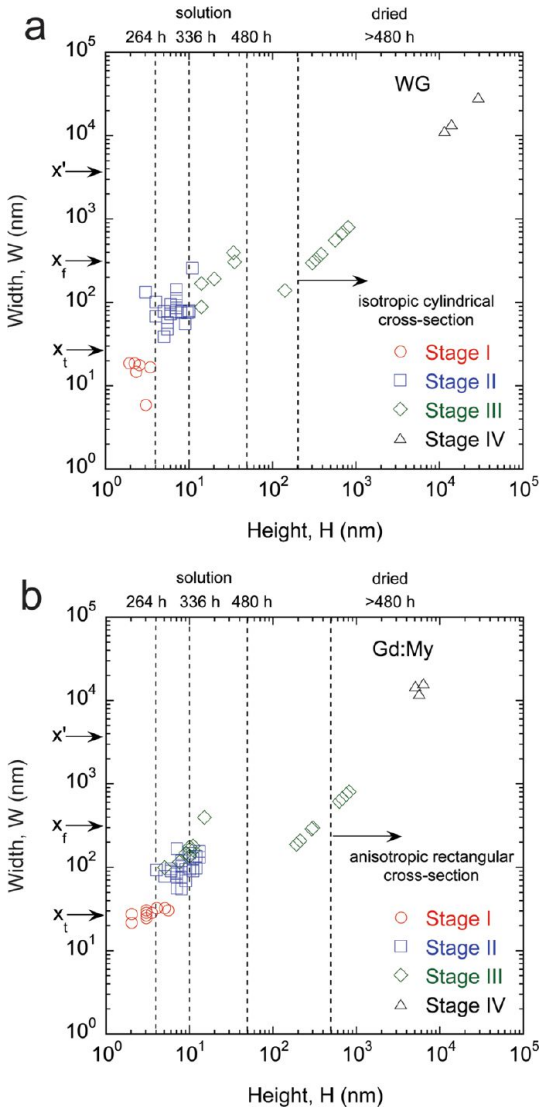

Figure 6. Growth of large self-assembled (a) WG peptide fibers and (b) Gd:My tapes with dimensions measured using AFM and SEM.

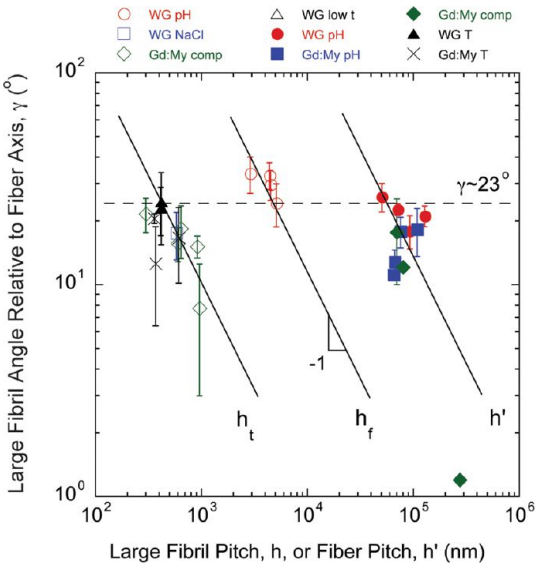

Figure 7. Fibers (h_f) and tapes (h_t) formed from WG and Gd:My peptides under various conditions separate based on morphological characteristics.

are observed in the dried tapes that are not observed in Stage III in solution (Figures 5 and 6b).

Micrometer-Sized Fiber Morphology. It is clear from the SEM images that fibers and tapes form from aggregates of large fibrils formed in Stage III. The large fibrils are oriented at an angle, γ, relative to the fiber or tape axis (Figure 4). At pH 8 and 37 °C, WG has $\gamma = 34°$ and Gd:My has $\gamma = 22°$ showing WG fibers to be more twisted and tightly packed (Figure 4). Therefore, the lateral aggregation of Gd:My fibrils induces a smaller twist than in WG. A transition from a tape to a cylinder morphology occurs at $\gamma \approx 23°$ and WG large fibrils can be prevented from twisting with changes in solution conditions.[75]

Concurrent with the orientation angle of the large fibrils is a pitch, h_f and h_t, for fibers and tapes, respectively.[40,62−64,66,78−80] For WG and Gd:My at pH 8 and 37 °C, $h_f = 2900$ nm and $h_t = 300$ nm, respectively, which defines the distance between large fibrils along the length of the micrometer-sized fiber or tape. Simple geometric considerations relate γ to h, $\gamma(°) = 360x/h$.[40,62−64,66,78−80,86] Measuring γ and h for WG and Gd:My mixtures studied under various experimental conditions shows that a plot of γ *versus* h segregates the resulting fibers and tapes by morphology regardless of peptide type or experimental condition (Figure 7).[35,75] In some cases, micrometer-sized fibers and tapes show very large scale twisting defined by a larger pitch, h'.[75] Fitting the data in Figure 7 to $\gamma(°) = 360x/h$ results in $x_t = 28$ nm, $x_f = 320$ nm, and $x' = 3.9$ μm. The length x_t is approximately equal to the protofibril width, which is the smallest discernible feature in the Gd:My tapes (Figure 5). x_f is approximately equal to the large fibril width, which is the smallest discernible feature in the WG fibers (Figure 4). It has been shown for protofibrils that the distance, x, is the distance between two peptides in the cross-β structure.[28,64,78,86] The peptides extend lengthwise across the width of the protofibril and when stacked side-by-side comprise the length of the protofibril. Protofibrils (in Gd:My) and large fibrils (in WG) organize side by side at an angle, γ, relative to the tape or fiber axis, respectively, thus x describes the smallest discernible feature comprising the tape or fiber length. x' is approximately equal to the final micrometer-sized fiber diameter and tape width. The x values span 2 orders of magnitude of scale (10^1−10^3 nm) and are length scales characteristic of the hierarchical nature of the self-assembly of micrometer-sized fibers and tapes.

In the simplest incarnation of the proposed multiscale self-assembly mechanism, hydrophobic interactions initiate template formation, the adder peptide addition, and aggregation of protofibrils into larger structures.[35,75] This is the path followed by Gd:My.

Myoglobin has large sequences of hydrophobic groups in its α-helices producing an α-helix hydrophobic content of 76%. Myoglobin only aggregates through hydrophobic interactions in certain portions of the protein which limits its solution phase aggregation to fibrils/large fibrils of dimensions H = 8−10 nm and W = 100−150 nm. Loosely bound protofibrils and fibrils are observed in the final dried Gd:My tapes, which have a Young's modulus of only $E_t \approx 0.15$ GPa. Lara *et al.* observe fibril aggregation similar to Stage III aggregation.[81] These "giant amyloid ribbons" resemble the Gd:My structures observed here and form from hydrolysates of hen egg white lysozyme and β-lactoglobulin with peptide molecular weights less than 6500 g/mol.[81] It is entirely possible that these hydrolysates contain peptides that meet "template" and "adder" definitions. That study also highlights the role of hydrophobic interactions in the lateral growth of the large tape.[66]

Myoglobin and GtL75 have similar aliphatic indices (AI), a measure of the molecular hydrophobicity.[35] However, glutenin peptides, specifically GtL75, contain glutamine repeat units or "Q-blocks" that are known facilitators of cross-β formation.[44,87−90] Myoglobin contains 4% Q without any Q-blocks. At short time, more protofibrils and fibrils form from WG globules than spontaneously form in Gd:My solution (Figure 1). Q-blocks appear to facilitate more early stage aggregation in WG through amide−amide hydrogen bonding on the amino acid side groups as measured with FT-IR spectroscopy.[35,75] This results in the more compact structure with smaller protofibril and fibril dimensions and higher rigidity manifesting as a longer persistence length in early stages. Experiments with short peptides containing Q-blocks have shown the resulting amyloid protofibrils to be more twisted than protofibrils formed from peptides of the same length without Q-blocks.[78] The Q-blocks facilitate twisting of the WG structures as seen in the AFM and SEM results and are responsible for morphological differentiation and a much higher Young's modulus of $E_f \approx 2.5$ GPa.[35,75] WG fibers have a longer pitch than Gd:My tapes. This appears to result from the more extensive formation of wider and thicker large fibrils in WG compared to Gd:My in Stage III and upon drying. Protofibrils and fibrils are assembled and twisted tightly in the WG large fibrils and are thus not the smallest discernible feature in WG fibers, unlike Gd:My tapes. The weaker hydrophobic interactions and lack of Q-Q bonding in Q-blocks do not allow twisting in the Gd:My system producing soft tapes rather than stiff cylinders.

CONCLUSION

Peptide mixtures can self-assemble into the often-studied nanometer scale amyloid protofibril and fibril. However, peptide mixtures with "template" and "adder" properties continue to assemble to the micrometer scale in a four-stage mechanism (Scheme 1). Hydrophobic adder proteins lacking Q-blocks, like My, have delayed and less extensive aggregation that rarely progresses past W = 150 nm in solution. Adder peptides with Q-blocks, like GtL75, facilitate aggregation through all four stages and cause twisting of the aggregating structure most notably at lengths greater than 100 nm. Most interestingly, the two peptide mixtures differentiate into two different morphologies. Differences in protofibril size and fibril persistence length appear in Stages I and II while stark morphological differences appear in Stages III and IV: a twisted cylindrical morphology for WG, containing GtL75, and a flat tape morphology for Gd:My. The twisted morphology from Q-blocks results in a fiber with a modulus 1 order of magnitude higher than that of the flat Gd:My tapes, which are built through weaker hydrophobic interactions only. An understanding of the peptide properties that dictate the progression and morphology of the large amyloid fiber indicates that it is possible to design a robust structure tailored to a specific function that exists on a length scale that lends itself to pragmatic engineering applications.

METHODS

Wheat Gluten (WG) and Gliadin (Gd) Hydrolysis and Self-Assembly. WG and Gd solutions were prepared in the same manner as previously described.[75] WG solution conditions were maintained at pH 8 and 37 °C for 20 days with samples collected periodically for AFM analysis.

Gd:My Solution. Gd:My solutions were made in the same manner as previously described.[75] Solution conditions were maintained at pH 8 and 37 °C with samples collected periodically for AFM analysis.

Atomic Force Microscopy (AFM). An amount of 50 μL of each solution was spin-coated on freshly cleaved mica at 4000 rpm for 1 min. Other studies have dried and washed their samples to reveal the amyloid fibrils on the mica surface. Spin-coating was used to immediately stop the self-assembly process and reveal the resulting amyloid structures to avoid a finite drying time that could have affected results.[64,66,81] Images were obtained with an Innova AFM (Bruker, Santa Barbara, CA) with a 0.01−0.025 Ohm-cm antimony-doped Si probe (Bruker, Part: MPP-1123-10) in tapping mode with a scan rate of 0.3 Hz. Images and measurements were evaluated using NanoScope Analysis v1.40 software. For dimensional measurements, the same image processing was performed for each figure. However, image contrast and clarity were enhanced with NanoScope Analysis v1.40 and Adobe Photoshop CS4 for the purposes of presentation. Dimension measurements of protofibrils (WG = 8, Gd:My = 11), fibrils (WG = 10, Gd:My = 18), large fibrils (WG = 5, Gd:My = 3) and fibers (WG, Gd:My = 3) were taken, and the averages ± standard deviations were reported. Multiple (at least 3) measurements were made on completely and partially separated protofibrils, fibrils, and large fibrils so that accurate heights and widths were reported. Fibers were measured once because of the uniformity of the cross-section and consistency with a more extensive previous study of fiber dimensions.[35]

Persistence length measurements were made as described previously.[63] Contour length and the angle between the tangents to both ends of the contour length were measured from the AFM images using ImageJ v1.46. The persistence length estimates were made on 17 WG and 13 Gd:My Stage II fibrils with averages ± standard deviations reported.

Scanning Electron Microscopy (SEM). WG and Gd:My solutions were dried on Teflon-coated aluminum foil under the fume hood at ambient conditions after 20 days. Fibers and tapes formed from dried solution were mounted onto aluminum SEM stubs with double-sided tape. Scanning electron micrographs were obtained using a LEO 1550 field-emission SEM (Zeiss, Peabody, MA) with a 4−6 mm working distance, 5 kV accelerating voltage, and an In-lens SE-detector.

Conflict of Interest: The authors declare no competing financial interest.

Acknowledgment. Generous funding through NSF-CMMI-0856262 and the USDA funded Virginia Tech Biodesign and Bioprocessing Research Center is gratefully acknowledged.

REFERENCES AND NOTES

1. Dobson, C. M. Protein Misfolding, Evolution and Disease. *Trends Biochem. Sci.* **1999**, *24*, 329–332.
2. Dobson, C. M.; Sali, A.; Darplus, M. Protein Folding: A Perspective from Theory and Experiment. *Angew. Chem., Int. Ed.* **1998**, *37*, 868–893.
3. Chiti, F.; Dobson, C. M. Protein Misfolding, Functional Amyloid, and Human Disease. *Annu. Rev. Biochem.* **2006**, *75*, 333–366.
4. Dobson, C. M. Protein Folding and Misfolding. *Nature* **2003**, *426*, 884–890.
5. Prusiner, S. B. Prions. *Proc. Natl. Acad. Sci. U.S.A.* **1998**, *95*, 13363–13383.
6. Paparcone, R.; Cranford, S. W.; Buehler, M. J. Self-Folding and Aggregation of Amyloid Nanofibrils. *Nanoscale* **2011**, *3*, 1748–1755.
7. Sunde, M. Common Core Structure of Amyloid Fibrils by Synchrotron X-ray Diffraction. *J. Mol. Biol.* **1997**, *273*, 729–739.
8. Hiramatsu, H.; Kitagawa, T. FT-IR Approaches on Amyloid Fibril Structure. *BBA-Proteins Proteom.* **2005**, *1753*, 100–107.
9. Knowles, T. P. J.; Buehler, M. J. Nanomechanics of Functional and Pathological Amyloid Materials. *Nat. Nanotechnol.* **2011**, *6*, 469–479.
10. Fowler, D. M.; Koulov, A. V.; Balch, W. E.; Kelly, J. W. Functional Amyloid—From Bacteria to Humans. *Trends Biochem. Sci.* **2007**, *32*, 217–224.
11. Kamino, K.; Odo, S.; Maruyama, T. Cement Proteins of the Acorn-Barnacle. *Megabalanus rosa. Biol. Bull.* **1996**, *190*, 403–409.
12. Kamino, K.; Inoue, K.; Maruyama, T.; Takamatsu, N.; Harayama, S.; Shizuri, Y. Barnacle Cement Proteins. *J. Biol. Chem.* **2000**, *275*, 27360–27365.
13. Kamino, K. Underwater Adhesive of Marine Organisms as the Vital Link between Biological Science and Material Science. *Mar. Biotechnol.* **2008**, *10*, 111–121.
14. Sullan, R. M. A.; Gunari, N.; Tanur, A. E.; Chan, Y.; Dickinson, G. H.; Orihuela, B.; Rittschof, D.; Walker, G. C. Nanoscale Structures and Mechanics of Barnacle Cement. *Biofouling* **2009**, *25*, 263–275.
15. Barlow, D. E.; Dickinson, G. H.; Orihuela, B.; Kulp, J. L., III; Rittschof, D.; Wahl, K. J. Characterization of the Adhesive Plaque of the Barnacle *Balanus amphitrite*: Amyloid-Like Nanofibrils are a Major Component. *Langmuir* **2010**, *26*, 6549–6556.
16. Gebbink, M. F. B. G.; Claessen, D.; Bouma, B.; Dijkhuizen, L.; Wosten, H. A. B. Amyloids—A Functional Coat for Microorganisms. *Nat. Rev. Microbiol.* **2005**, *3*, 333–341.
17. Ben Nasr, A.; Olsen, A.; Sjobring, U.; Muller-Esterl, W.; Bjorck, L. Assembly of Human Contact Phase Proteins and Release of Bradykinin at the Surface of Curli-Expressing *Escheria coli*. *Mol. Microbiol.* **1996**, *20*, 927–935.
18. Hammer, N. D.; Schmidt, J. C.; Chapman, M. R. The Curli Nucleator Protein, CsgB, Contains an Amyloidogenic Domain that Directs CsgA Polymerization. *Proc. Natl. Acad. Sci. U.S.A.* **2007**, *104*, 12494–12499.
19. Wang, X.; Chapman, M. R. Curli Provide the Template for Understanding Controlled Amyloid Propagation. *Prion* **2008**, *2*, 57–60.
20. Wang, X.; Hammer, N. D.; Chapman, M. R. The Molecular Basis of Functional Bacterial Amyloid Polymerization and Nucleation. *J. Biol. Chem.* **2008**, *283*, 21530–21539.
21. Chapman, M. R.; Robinson, L. S.; Pinkner, J. S.; Roth, R.; Heuser, J.; Hammar, M.; Normark, S.; Hultgren, S. J. Role of *Escherichia coli* Curli Operons in Directing Amyloid Fiber Formation. *Science* **2002**, *295*, 851–855.
22. Alsteens, D.; Ramsook, C. B.; Lipke, P. N.; Dufrêne, Y. F. Unzipping a Functional Microbial Amyloid. *ACS Nano* **2012**, *6*, 7703–7711.
23. Parker, K. D.; Rudall, K. M. The Silk of the Egg-Stalk of the Green Lace-Wing Fly. *Nature* **1957**, *179*, 905–906.
24. Weisman, S.; Trueman, H. E.; Mudie, S. T.; Church, J. S.; Sutherland, T. D.; Haritos, V. S. An Unlikely Silk: The Composite Material of Green Lacewing Cocoons. *Biomacromolecules* **2008**, *9*, 3065–3069.
25. Seidel, A.; Liivak, O.; Calve, S.; Adaska, J.; Ji, G.; Yang, Z.; Grubb, D.; Zax, D. B.; Jelinski, L. W. Regenerated Spider Silk: Processing, Properties, and Structure. *Macromolecules* **2000**, *33*, 775–780.
26. Keten, S.; Xu, Z.; Ihle, B.; Buehler, M. J. Nanoconfinement Controls Stiffness, Strength and Mechanical Toughness of β-Sheet Crystals in Silk. *Nat. Mater.* **2010**, *9*, 359–367.
27. Xu, Z.; Paparcone, R.; Buehler, M. J. Alzheimer's Aβ(1−40) Amyloid Fibrils Feature Size-Dependent Mechanical Properties. *Biophys. J.* **2010**, *98*, 2053–2062.
28. Paparcone, R.; Keten, S.; Buehler, M. J. Atomistic Simulation of Nanomechanical Properties of Alzheimer's Aβ(1−40) Amyloid Fibrils under Compressive and Tensile Loading. *J. Biomech.* **2010**, *43*, 1196–1201.
29. Fukuma, T.; Mostaert, A.; Jarvis, S. Explanation for the Mechanical Strength of Amyloid Fibrils. *Tribol. Lett.* **2006**, *22*, 233–237.
30. Knowles, T. P. J.; Oppenheim, T. W.; Buell, A. K.; Chirgadze, D. Y.; Welland, M. E. Nanostructured Films from Hierarchical Self-Assembly of Amyloidogenic Proteins. *Nat. Nanotechnol.* **2010**, *5*, 204–207.
31. Li, C.; Adamcik, J.; Mezzenga, R. Biodegradable Nanocomposites of Amyloid Fibrils and Graphene with Shape-Memory and Enzyme-Sensing Properties. *Nat. Nanotechnol.* **2012**, *7*, 421–427.
32. Gazit, E. Self-Assembled Peptide Nanostructures: The Design of Molecular Building Blocks and Their Technological Utilization. *Chem. Soc. Rev.* **2007**, *32*, 1263–1269.
33. Reches, M.; Gazit, E. Casting Metal Nanowires within Discrete Self-Assembled Peptide Nanotubes. *Science* **2003**, *300*, 625–627.
34. Scheibel, T.; Parthasarathy, R.; Sawicki, G.; Lin, X. M.; Jaeger, H.; Lindquist, S. L. Conducting Nanowires Built by Controlled Self-Assembly of Amyloid Fibers and Selective Metal Deposition. *Proc. Natl. Acad. Sci. U.S.A.* **2003**, *100*, 4527–4532.
35. Ridgley, D. M.; Ebanks, K. C.; Barone, J. R. Peptide Mixtures Can Self-Assemble into Large Amyloid Fibers of Varying Size and Morphology. *Biomacromolecules* **2011**, *12*, 3770–3779.
36. Athamneh, A.; Barone, J. R. Enzyme-Mediated Self-Assembly of Highly Ordered Structures from Disordered Proteins. *Smart Mater. Struct.* **2009**, *18*, 104024.
37. Bouchard, M.; Zurdo, J.; Nettleton, E. J.; Dobson, C. M.; Robinson, C. V. Formation of Insulin Amyloid Fibrils followed by FT-IR Simultaneously with CD and Electron Microscopy. *Protein Sci.* **2000**, *9*, 1960–1967.
38. Gosal, W. S.; Morten, I. J.; Hewitt, E. W.; Smith, A.; Thomson, N. H.; Radford, S. E. Competing Pathways Determine Fibril Morphology in the Self-Assembly of β_2-Microglobulin into Amyloid. *J. Mol. Biol.* **2005**, *351*, 850–864.

39. Fandrich, M.; Fletcher, M. A.; Dobson, C. M. Amyloid Fibrils from Muscle Myoglobin. *Nature* **2001**, *410*, 165–166.
40. Davies, R. P. W.; Aggeli, A.; Beevers, A. J.; Boden, N.; Carrick, L. M.; Fishwick, C. W. G.; McLeish, T. C. B.; Nyrkova, I. A.; Semenov, A. N. Self-Assembling β-sheet Tape Forming Peptides. *Supramol. Chem.* **2006**, *18*, 435–443.
41. Barghorn, S.; Davies, P.; Mandelkow, E. Tau Paired Helical Filaments from Alzheimer's Disease Brain and Assembled *in Vitro* Are Based on β-Structure in the Core Domain. *Biochemistry U.S.* **2004**, *43*, 1694–1703.
42. Hasegawa, K.; Yamaguchi, I.; Omata, S.; Gejyo, F.; Naiki, H. Interaction between Aβ(1−42) and Aβ(1−40) in Alzheimer's β-Amyloid Fibril Formation *in Vitro*. *Biochemistry U.S.* **1999**, *38*, 15514–15521.
43. Ivanova, M. I.; Sawaya, M. R.; Gingery, M.; Attinger, A.; Eisenberg, D. An Amyloid-Forming Segment of β2-Microglobulin Suggests a Molecular Model for the Fibril. *Proc. Natl. Acad. Sci. U.S.A.* **2004**, *101*, 10584–10589.
44. Chen, S.; Berthelier, V.; Bradley Hamilton, J.; O'Nuallain, B.; Wetzel, R. Amyloid-like Features of Polyglutamine Aggregates and Their Assembly Kinetics. *Biochemistry U.S.* **2002**, *41*, 7391–7399.
45. Cherny, I.; Gazit, E. Amyloids: Not Only Pathological Agents but Also Ordered Nanomaterials. *Angew. Chem., Int. Ed.* **2008**, *47*, 4062–4069.
46. Cohen, A. S.; Calkins, E. Electron Microscopic Observations on a Fibrous Component in Amyloid of Diverse Origins. *Nature* **1959**, *183*, 1202–1203.
47. del Mercato, L. L.; Maruccio, G.; Pompa, P. P.; Bochiccio, B.; Tamburro, A. M.; Cingolani, R.; Rinaldi, R. Amyloid-like Fibrils in Elastin-Related Polypeptides: Structural Characterization and Elastic Properties. *Biomacromolecules* **2008**, *9*, 796–803.
48. Diaz-Avalos, R. Cross-β Order and Diversity in Nanocrystals of an Amyloid-Forming Peptide. *J. Mol. Biol.* **2003**, *330*, 1165–1175.
49. Eanes, E. D.; Glenner, G. G. X-ray Diffraction Studies on Amyloid Filaments. *J. Histochem. Cytochem.* **1968**, *16*, 673–677.
50. Gosal, W. S.; Clark, A. H.; Pudney, P. D. A.; Ross-Murphy, S. B. Novel Amyloid Fibrillar Networks Derived from a Globular Protein: β-Lactoglobulin. *Langmuir* **2002**, *18*, 7174–7181.
51. Jaroniec, C. P.; MacPhee, C. E.; Astrof, N. S.; Dobson, C. M.; Griffin, R. G. Molecular Conformation of a Peptide Fragment of Transthyretin in an Amyloid Fibril. *Proc. Natl. Acad. Sci. U.S.A.* **2002**, *99*, 16748–16753.
52. Jimenez, J. L. Cryo-electron Microscopy Structure of an SH3 Amyloid Fibril and Model of the Molecular Packing. *EMBO J.* **1999**, *18*, 815–821.
53. Jimenez, J. L. The Protofilament Structure of Insulin Amyloid Fibrils. *Proc. Natl Acad. Sci. U.S.A.* **2002**, *99*, 9196–9201.
54. MacPhee, C. E.; Dobson, C. M. Formation of Mixed Fibrils Demonstrates the Generic Nature and Potential Utility of Amyloid Nanostructures. *J. Am. Chem. Soc.* **2000**, *122*, 12707–12713.
55. Pearce, F. G.; Mackintosh, S. H.; Gerrard, J. A. Formation of Amyloid-like Fibrils by Ovalbumin and Related Proteins under Conditions Relevant to Food Processing. *J. Agric. Food Chem.* **2007**, *55*, 318–322.
56. Perutz, M. F.; Finch, J. T.; Berriman, J.; Lesk, A. Amyloid Fibers Are Water-Filled Nanotubes. *Proc. Natl. Acad. Sci. U.S.A.* **2002**, *99*, 5591–5595.
57. Petkova, A. T. A Structural Model for Alzheimer's β-Amyloid Fibrils based on Experimental Constraints from Solid State NMR. *Proc. Natl. Acad. Sci. U.S.A.* **2002**, *99*, 16742–16747.
58. Rubin, N.; Perugia, E.; Goldschmidt, M.; Fridkin, M.; Addadi, L. Chirality of Amyloid Suprastructures. *J. Am. Chem. Soc.* **2008**, *130*, 4602–4603.
59. Sunde, M.; Blake, C. C. F. From the Globular to the Fibrous State: Protein Structure and Structural Conversion in Amyloid Formation. *Q. Rev. Biophys.* **1998**, *31*, 1–39.
60. Torok, M. Structural and Dynamic Features of Alzheimer's Aβ Peptide in Amyloid Fibrils Studied by Site-Directed Spin Labeling. *J. Biol. Chem.* **2002**, *277*, 40810–40815.
61. Zurdo, J.; Guijarro, J. I.; Dobson, C. M. Preparation and Characterization of Purified Amyloid Fibrils. *J. Am. Chem. Soc.* **2001**, *123*, 8141–8142.
62. Adamcik, J.; Berquand, A.; Mezzenga, R. Single-Step Direct Measurement of Amyloid Fibrils Stiffness by Peak Force Quantitative Nanomechanical Atomic Force Microscopy. *Appl. Phys. Lett.* **2011**, *98*, 193701.
63. Adamcik, J.; Jung, J. M.; Flakowski, J.; De Los Rios, P.; Dietler, G.; Mezzenga, R. Understanding Amyloid Aggregation by Statistical Analysis of Atomic Force Microscopy Images. *Nat. Nanotechnol.* **2010**, *5*, 423–428.
64. Adamcik, J.; Mezzenga, R. Adjustable Twisting Periodic Pitch of Amyloid Fibrils. *Soft Matter* **2011**, *7*, 5437–5443.
65. Bolder, S. G.; Hendrickx, H.; Sagis, L. M. C.; van der Linden, E. Fibril Assemblies in Aqueous Whey Protein Mixtures. *J. Agric. Food Chem.* **2006**, *54*, 4229–4234.
66. Bolisetty, S.; Adamcik, J.; Mezzenga, R. Snapshots of Fibrillation and Aggregation Kinetics in Multistranded Amyloid β-Lactoglobulin Fibrils. *Soft Matter* **2011**, *7*, 493–499.
67. Fandrich, M.; Forge, V.; Buder, K.; Kittler, M.; Dobson, C. M.; Diekmann, S. Myoglobin forms Amyloid Fibrils by Association of Unfolded Polypeptide Segments. *Proc. Natl. Acad. Sci. U.S.A.* **2003**, *100*, 15463–15468.
68. Goda, S.; Takano, K.; Yamagata, Y.; Nagata, R.; Akutsu, H.; Maki, S.; Namba, K.; Yutani, K. Amyloid Protofilament Formation of Hen Egg Lysozyme in Highly Concentrated Ethanol Solution. *Protein Sci.* **2000**, *9*, 369–375.
69. Mostaert, A.; Higgins, M. J.; Fukuma, T.; Rindi, F.; Jarvis, S. P. Nanoscale Mechanical Characterization of Amyloid Fibrils Discovered in a Natural Adhesive. *J. Biol. Phys.* **2006**, *32*, 393–401.
70. Tomaselli, S.; Esposito, V.; Vangone, P.; van Nuland, N. A. J.; Bonvin, A. M. J. J.; Guerrini, R.; Tancredi, T.; Temussi, P. A.; Picone, D. The α-to-β Conformational Transition of Alzheimer's Aβ-(1−42) Peptide in Aqueous Media is Reversible: A Step by Step Conformational Analysis Suggests the Location of β Conformation Seeding. *ChemBioChem* **2006**, *7*, 257–267.
71. Jarrett, J. T.; Lansbury, P. T. Amyloid Fibril Formation Requires a Chemically Discriminating Nucleation Event: Studies of an Amyloidogenic Sequence from the Bacterial Protein OsmB. *Biochemistry* **1992**, *31*, 12345–12352.
72. Ionescu-Zanetti, C.; Khurana, R.; Gillespie, J. R.; Petrick, J. S.; Trabachino, L. C.; Minert, L. J.; Carter, S. A.; Fink, A. L. Monitoring the Assembly of Ig Light-Chain Amyloid Fibrils by Atomic Force Microscopy. *Proc. Natl. Acad. Sci. U.S.A.* **1999**, *96*, 13175–13179.
73. Chamberlain, A. K.; MacPhee, C. E.; Zurdo, J.; Morozova-Roche, L. A.; Hill, H. A. O.; Dobson, C. M.; Davis, J. J. Ultrastructural Organization of Amyloid Fibrils by Atomic Force Microscopy. *Biophys. J.* **2000**, *79*, 3282–3293.
74. Sweers, K. K. M.; van der Werf, K. O.; Bennink, M. L.; Subramaniam, V. Atomic Force Microscopy under Controlled Conditions Reveals Structure of C-Terminal Region of α-Synuclein in Amyloid Fibrils. *ACS Nano* **2012**, *6*, 5952–5960.
75. Ridgley, D. M.; Claunch, E. C.; Barone, J. R. The Effect of Processing on Large, Self-Assembled Amyloid Fibers. *Soft Matter* **2012**, *8*, 10298–10306.
76. Raman, B.; Chatani, E.; Kihara, M.; Ban, T.; Sakai, M.; Hasegawa, K.; Naiki, H.; Rao, C. M.; Goto, Y. Critical Balance of Electrostatic and Hydrophobic Interactions Is Required for β2-Microglobulin Amyloid Fibril Growth and Stability. *Biochemistry* **2005**, *44*, 1288–1299.
77. Kodali, R.; Williams, A. D.; Chemuru, S.; Wetzel, R. Aβ(1−40) Forms Five Distinct Amyloid Structures Whose β-Sheet Contents and Fibril Stabilities Are Correlated. *J. Mol. Biol.* **2010**, *401*, 503–517.
78. Aggeli, A.; Nyrkova, I. A.; Bell, M.; Harding, R.; Carrick, L.; McLeish, T. C. B.; Semenov, A. N.; Boden, N. Hierarchical Self-Assembly of Chiral Rod-like Molecules as a Model for Peptide β-Sheet Tapes, Ribbons, Fibrils, and Fibers. *Proc. Natl. Acad. Sci. U.S.A.* **2001**, *98*, 11857–11862.
79. Nyrkova, I. A.; Semenov, A. N.; Aggeli, A.; Bell, M.; Boden, N.; McLeish, T. C. B. Self-Assembly and Structure Formation in

Living Polymers Forming Fibrils. *Euro. Phys. J. B* **2000**, *17*, 499–513.
80. Nyrkova, I. A.; Semenov, A. N.; Aggeli, A.; Boden, N. Fibril Stability in Solutions of Twisted β-Sheet Peptides: A New Kind of Micellization in Chiral Systems. *Euro. Phys. J. B* **2000**, *17*, 481–497.
81. Lara, C.; Adamcik, J.; Jordens, S.; Mezzenga, R. General Self-Assembly Mechanism Converting Hydrolyzed Globular Proteins Into Giant Multistranded Amyloid Ribbons. *Biomacromolecules* **2011**, *12*, 1868–1875.
82. Ban, T.; Yamaguchi, K.; Goto, Y. Direct Observation of Amyloid Fibril Growth, Propagation, and Adaptation. *Acc. Chem. Res.* **2006**, *39*, 663–670.
83. Jarrett, J. T.; Lansbury, P. T. Seeding "One-Dimensional Crystallization" of Amyloid: A Pathogenic Mechanism in Alzheimer's Disease and Scrapie? *Cell* **1993**, *73*, 1055–1058.
84. Keller, A.; Fritzsche, M.; Yu, Y. P.; Liu, Q.; Li, Y. M.; Dong, M.; Besenbacher, F. Influence of Hydrophobicity on the Surface-Catalyzed Assembly of the Islet Amyloid Polypeptide. *ACS Nano* **2011**, *5*, 2770–2778.
85. Lashuel, H. A.; LaBrenz, S. R.; Woo, L.; Serpell, L. C.; Kelly, J. W. Protofilaments, Filaments, Ribbons, and Fibrils from Peptidomimetic Self-Assembly: Implications for Amyloid Fibril Formation and Materials Science. *J. Am. Chem. Soc.* **2000**, *122*, 5262–5277.
86. Paparcone, R.; Buehler, M. J. Microscale Structural Model of Alzheimer Aβ(1−40) Amyloid Fibril. *Appl. Phys. Lett.* **2009**, *94*, 243904–3.
87. Perutz, M. F.; Johnson, T.; Suzuki, M.; Finch, J. T. Glutamine Repeats as Polar Zippers: Their Possible Role in Inherited Neurodegenerative Diseases. *Proc. Natl. Acad. Sci. U.S.A.* **1994**, *91*, 5355–5358.
88. DePace, A. H.; Santoso, A.; Hillner, P.; Weissman, J. S. A Critical Role for Amino-Terminal Glutamine/Asparagine Repeats in the Formation and Propagation of a Yeast Prion. *Cell* **1998**, *93*, 1241–1252.
89. Scherzinger, E.; Sittler, A.; Schweiger, K.; Heiser, V.; Lurz, R.; Hasenbank, R.; Bates, G. P.; Lehrach, H.; Wanker, E. E. Self-Assembly of Polyglutamine-Containing Huntingtin Fragments into Amyloid-like Fibrils: Implications for Huntington's Disease Pathology. *Proc. Natl. Acad. Sci. U.S.A.* **1999**, *96*, 4604–4609.
90. Sikorski, P.; Atkins, E. New Model for Crystalline Polyglutamine Assemblies and Their Connection with Amyloid Fibrils. *Biomacromolecules* **2005**, *6*, 425–432.